Two-dimensional molecular *para*-hydrogen and *ortho*-deuterium at zero temperature

C. Cazorla[1,2,3] and J. Boronat[4]
[1]*London Centre for Nanotechnology, UCL, London WC1H OAH, United Kingdom*
[2]*Department of Physics and Astronomy, UCL, London WC1E 6BT, United Kingdom*
[3]*Materials Simulation Laboratory, London WC1E 6BT, United Kingdom*
[4]*Departament de Física i Enginyeria Nuclear, UPC, Campus Nord B4-B5, E-08034 Barcelona, Spain*
(Received 4 June 2008; revised manuscript received 4 September 2008; published 8 October 2008)

We study molecular *para*-hydrogen (p-H_2) and *ortho*-deuterium (o-D_2) in two dimensions and in the limit of zero temperature by means of the diffusion Monte Carlo method. We report energetic and structural properties of both systems such as the total and kinetic energy per particle, radial pair distribution function, and Lindemann's ratio in the low-pressure regime. By comparing the total energy per particle as a function of the density in liquid and solid p-H_2, we show that molecular *para*-hydrogen, and also *ortho*-deuterium, remains solid at zero temperature. Interestingly, we assess the quality of three different symmetrized trial wave functions, based on the Nosanow-Jastrow model, in the p-H_2 solid film at the variational level. In particular, we analyze one type of symmetrized trial wave function which has been used very recently to describe solid ^{4}He and found that it also characterizes hydrogen satisfactorily. Using this trial wave function, we estimate the one-body density matrix $\varrho_1(r)$ of solid p-H_2 at several densities close to equilibrium and find off-diagonal long-range order with a condensate fraction n_0 that increases sizably in the regime of negative pressures. The extrapolated estimation of n_0 is observed to depend on the form of the symmetrized trial wave function used for importance sampling however the corresponding order of magnitude remains the same in all the cases. We have also computed the superfluid fraction ρ_s/ρ of two-dimensional solid p-H_2 at zero temperature in an unbiased way and found that it is nonzero at negative pressures.

DOI: 10.1103/PhysRevB.78.134509 PACS number(s): 67.80.−s, 67.90.+z, 61.50.Ah

I. INTRODUCTION

Quantum crystals such as helium and hydrogen are intriguing systems of fundamental physical interest. Due to the light mass of their constituents and relatively weak interparticle attraction, quantum solids exhibit large kinetic energy and Lindemann's ratio even in the limit of zero temperature ($T \sim 10^0 - 10^{-3}$ K). In consequence, anharmonic effects and atomic quantum exchanges are of importance in this class of crystals. Moreover, in the last few years a series of ultralow-temperature experiments performed in solid ^{4}He by different groups has led to a renewed interest on the possibility of superfluidity and/or Bose-Einstein condensation (BEC) in quantum solids.[1–4] Essentially, these experiments analyze the quantum behavior of the helium crystal upon rotation or seek for some thermodynamic and/or structural anomaly signalizing a possible normal-to-superfluid phase transition. Despite that most of the observations fairly agree in locating the onset of superfluidity (75–150 mK), there is a large dispersion in the value of the measured superfluid fraction $\rho_s/\rho (\simeq 0.3\% - 0.005\%)$. At present, there is lack of conclusive arguments for explaining these discrepancies but it is widely accepted that the purity of the sample and the presence of crystalline defects play on it a relevant role.[5,6] On the other hand, there is overall agreement among microscopic full quantum calculations in practically ruling out superfluidity in the perfect (free of defects) bulk configuration. It is worth noticing that usual techniques devised to study classical crystals (that is, crystals composed of heavier elements and with larger cohesive energies)—such as, for instance, harmonic based approaches—are no longer suitable for quantum solids and calculations on them are in most cases challenging.[7,8]

In the present work, we present a theoretical study of two-dimensional (2D) molecular *para*-hydrogen (p-H_2) and *ortho*-deuterium (o-D_2) at zero temperature by means of the diffusion Monte Carlo (DMC) method[9–11] and the semiempirical radial pair interaction due to Silvera and Goldman.[12] Hydrogen is a very interesting and challenging system which has been investigated very intensively during the last half century. As a matter of fact, hydrogen is the most abundant element in the universe and from a technological point of view it is considered among the most promising green combustibles of the near future. Very interestingly, hydrogen has been predicted to exhibit a new state of matter at very high pressures ($P \sim 400$ GPa) in which superfluidity and superconductivity might coexist.[13,14]

In this work, we restrict our analysis of molecular hydrogen and deuterium to the low-pressure regime ($P \sim 0$) and zero temperature. Contrarily to what occurs in helium, molecular hydrogen freezes at a temperature of 13.96 K in spite of its lighter mass, given that the interactions between particles are more attractive (the minimum of the interaction between hydrogen molecules amounts to ~ -37 K while in helium it is ~ -10 K). One of our motivations for carrying out the present study was to unravel whether liquid p-H_2 could be stabilized or not at zero temperature by reducing the dimensionality with respect to the bulk. This possibility appears to be very appealing since it would provide a chance for superfluidity and BEC to be observed in a quantum liquid different from helium. In fact, p-H_2 in one dimension and inside a carbon nanotube has already been studied in the zero-temperature limit and predicted to be liquid at its equilibrium density.[15] Also, small drops with a number of molecules $N \lesssim 26$ present superfluid character.[16–18] On the other hand, it has been reported recently an experiment performed

on molecular *ortho*-deuterium preplated on krypton at very low temperatures ($T \sim 1$ K) in which it is claimed evidence for the existence of a reentrant o-D_2 liquid phase.[19] As it will be presented in short, our results show that no first-order solid-liquid phase transition occurs in two-dimensional H_2 at zero temperature. On account of this result, we straightforwardly reject this possibility also for o-D_2 since deuterium molecules are heavier and their intermolecular interactions are considered equal to the H_2-H_2 ones. Consequently, most of the effort done in this work has been devoted to achieve an accurate description of the ground state of two-dimensional solid p-H_2 and o-D_2.

In this work, we calculate by means of the DMC method some energetic and structural properties of both hydrogen and deuterium films near equilibrium. Quantities such as the kinetic energy per particle and Lindemann's ratio have been computed within the pure estimator approach[20–22] in order to remove any possible bias coming out from the trial wave function (TWF) used for importance sampling. In this way, we quote quantum isotopic effects in hydrogen directly and only within the statistical uncertainty. Previous to the DMC results, we present a variational Monte Carlo (VMC) study of the p-H_2 crystal in which we have tested the quality of several symmetrized and unsymmetrized trial wave functions. With this analysis, we determine the effect of symmetrization on the total energy and the relevance of molecule exchanges along the simulation. Moreover, we analyze which symmetrized wave functions can be implemented in DMC to the end of estimating the possible superfluidity and BEC of the solid with simultaneous accurate description of their energetic and structural properties. In particular, we have studied in detail a symmetrized trial wave function, named ψ_{JG}^{S3} in this work (the notation will become clear later), which has been proposed and used recently to study bulk solid ^{4}He.[23] Here, we find that ψ_{JG}^{S3} also characterizes solid hydrogen in two dimensions accurately.

Interestingly, we assess the behavior of the one-body density matrix $\varrho_1(r)$ of p-H_2 with density by means of the symmetric trial wave function ψ_{JG}^{S3}. In all cases, a very small condensate fraction n_0 is observed. For densities below the equilibrium one and near the spinodal point, a significant increase in n_0 is observed pointing to the emergence of a finite superfluid density.

This paper is organized as follows. In Sec. II, we present a brief description of the semiempirical pair potential and techniques used throughout this work. Next, in Secs. III and IV, we report our variational and diffusion Monte Carlo results for p-H_2 and o-D_2 in two dimensions, respectively. Section V is devoted to the examination of the one-body density matrix $\varrho_1(r)$ obtained with ψ_{JG}^{S3} and its dependence with the density. Finally, in Sec. VI we summarize the main results presented in this work.

II. MOLECULAR INTERACTION AND METHOD

The H_2 (D_2) molecule is composed of two hydrogen (deuterium) atoms linked by a covalent bond, which in the *para*-hydrogen (*ortho*-deuterium) state possesses spherical symmetry (zero total angular momentum). The energy scale involved in electronic excitations ($\sim 10^5$ K) is orders of magnitude larger than the intermolecular one ($\sim 10^1$ K); thus to model the H_2-H_2 (or D_2-D_2) interaction by means of a radial pair potential and consider the molecules as pointlike turn out to be justified upon the condition of low or moderate pressures. In this work, we have adopted the well-known and commonly used semiempirical Silvera-Goldman pair potential.[12] This potential has proved to perform excellently at low temperature and at the pressure regimes in which we are interested.

The ground state of *para*-H_2 and *ortho*-D_2 is determined using the DMC method. DMC is a zero-temperature method which provides the exact ground-state energy of many-boson interacting systems within some statistical uncertainty.[9–11] This technique is based on a short-time approximation for Green's function corresponding to the imaginary time (τ)-dependent Schrödinger equation. Despite this method is algorithmically simpler than domain Green's-function Monte Carlo,[11,24] it presents some $(\Delta\tau)^n$ bias coming from the factorization of the imaginary time propagator $e^{-(\Delta\tau/\hbar)H}$. Our implementation of DMC is quadratic,[25] hence the control of the time-step bias is efficiently controlled given that the required $\Delta\tau \to 0$ extrapolation is nearly eliminated by choosing a sufficiently small time step. The Hamiltonian H describing our system is

$$H = -\frac{\hbar^2}{2m}\sum_{i=1}^{N}\nabla_i^2 + \sum_{i<j}^{N} V(r_{ij}), \tag{1}$$

and the corresponding Schrödinger equation in imaginary time ($it \equiv \tau$)

$$-\hbar\frac{\partial\Psi(\mathbf{R},\tau)}{\partial\tau} = (H-E)\Psi(\mathbf{R},\tau), \tag{2}$$

with E as an arbitrary constant. Equation (2) can be formally solved by expanding the solution $\Psi(\mathbf{R},\tau)$ in the basis set of the energy eigenfunctions $\{\Phi_n\}$ ($\mathbf{R} \equiv \{\mathbf{r}_1, \mathbf{r}_2, \ldots, \mathbf{r}_N\}$). It turns out that $\Psi(\mathbf{R},\tau)$ tends to the ground-state wave function Φ_0 of the system for an infinite imaginary time as well as the expected value of the Hamiltonian tends to the ground-state value E_0. The Hermiticity of the Hamiltonian guarantees the equality,

$$E_0 = \frac{\langle\Phi_0|H|\Phi_0\rangle}{\langle\Phi_0|\Phi_0\rangle} = \frac{\langle\Phi_0|H|\psi_T\rangle}{\langle\Phi_0|\psi_T\rangle} = \langle H\rangle_{\mathrm{DMC}}, \tag{3}$$

where ψ_T is a convenient trial wave function. As a consequence, the ground-state energy of the system can be computed by calculating the integral,

$$\langle H\rangle_{\mathrm{DMC}} = \lim_{\tau\to\infty}\int_V E_L(\mathbf{R}) f(\mathbf{R},\tau) d\mathbf{R}, \tag{4}$$

where $f(\mathbf{R},\tau) = \Psi(\mathbf{R},\tau)\psi_T(\mathbf{R})$ and $E_L(\mathbf{R})$ is the local energy defined as $E_L(\mathbf{R}) = H\psi_T(\mathbf{R})/\psi_T(\mathbf{R})$. The introduction of $\psi_T(\mathbf{R})$ in $f(\mathbf{R},\tau)$ is known as importance sampling and its use is important to reduce the variance of Eq. (4) to a manageable level [for instance, by imposing $\psi_T(\mathbf{R}) = 0$ when r_{ij} is smaller than the core of the pair interaction].

In this work, all the operators diagonal in real space which do not commute with the Hamiltonian, which is $[H,\hat{O}] \neq 0$, have been sampled using the pure estimator technique based on forward walking.[20–22] Essentially, with this method the possible bias introduced by ψ_T in the mixed estimator $\langle \Phi_0 | \hat{O} | \psi_T \rangle$ is removed by proper weighing of the configurations generated along the simulation.

III. MOLECULAR *PARA*-HYDROGEN

A. Variational Monte Carlo results

In this section, we present a VMC study of two-dimensional p-H_2 which provides us with the most convenient TWF to be used in subsequent DMC calculations and valuable physical insight on the system itself. In brief, the VMC method relies on the variational principle which states that given a Hamiltonian the energy difference $E_L - E_0$ averaged over the probability density distribution $|\psi_T|^2$ is always positive and it decreases as the overlapping between ψ_T and the true ground-state wave function increases (E_L and E_0 are the local energy defined in Sec. II and the ground-state energy, respectively). In the present work, the main variational effort has been devoted to achieve an accurate description of the 2D solid phase. We have checked by means of VMC and DMC that in both p-H_2 and o-D_2 systems the triangular configuration is the stable one at all the studied densities. The energies reported in this section have been calculated at the density $\rho = 0.060$ Å^{-2}, which corresponds to the variational equilibrium density of the solid.

In order to determine the nature of the ground state of the system we have also carried out simulations for the liquid phase. In this case, the trial wave function is of Jastrow type,

$$\psi_J(\mathbf{r}_1, \mathbf{r}_2, \ldots, \mathbf{r}_N) = \prod_{i<j}^{N} f_2(r_{ij}), \tag{5}$$

where the two-body factors f_2 account for the molecular correlations arising in the system due to pair interactions. These two-body correlation factors have been chosen of McMillan form, $f_2 = e^{-(1/2)(b/r)^5}$, and as best value of the variational parameter b we obtain 3.70 Å.

For the solid phase, an additional one-body factor is introduced *ad hoc* in the trial wave function to the end of reproducing the periodic order of the system and so making the sampling over the space of configurations more efficient (Nosanow-Jastrow model). Such one-body factor consists in a productory of localizing functions centered on the positions that define the perfect-crystal configuration (sites), given by the family of vectors $\{\mathbf{R}_i\}$,

$$\psi_{NJ}(\mathbf{r}_1, \mathbf{r}_2, \ldots, \mathbf{r}_N) = \psi_J \prod_{i}^{N} g_1(|\mathbf{r}_i - \mathbf{R}_i|). \tag{6}$$

We have explored two different trial wave functions based on ψ_{NJ}, each one consisting in a different choice for $g_1(r)$. The first model corresponds to the standardly used Gaussian function,

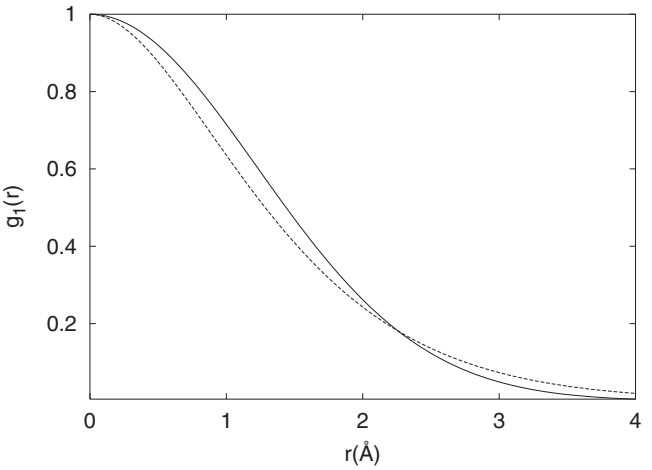

FIG. 1. Optimized Gaussian and Padé functions (solid and dashed line, respectively) for solid p-H_2 at the density $\rho = 0.060$ Å^{-2}. The decay of $g_P(r)$ to zero is smoother than that of $g_G(r)$, and in the region around the origin $g_P(r)$ is narrower.

$$g_G(r) = \exp\left(-\frac{a_G}{2} r^2\right), \tag{7}$$

while the second is a Padé function, defined as

$$g_P(r) = \exp\left(-\frac{a_P r^2}{1 + c_P r}\right), \tag{8}$$

where a_G, a_P, and c_P are variational parameters to be optimized. Even though $g_G(r)$ and $g_P(r)$ are analytically quite similar, the decay of g_P to zero at large distance r can be chosen to be less abrupt than that of $g_G(r)$ (see Fig. 1). This feature can be used in the simulations for increasing somewhat the degree of delocalization of the molecules at the expense, however, of an increase in the kinetic energy within the surroundings of the equilibrium positions [where $g_P(r)$ varies more rapidly than $g_G(r)$]. In Table I, we report the best energies obtained in the optimization process of ψ_{NJ} with Gaussian and Padé functions for $g_1(r)$ as well as the optimal set of parameters. As one can see, in both cases the lowest energy obtained is −21.3(1) K. It is worthwhile noticing that when the asymptotes of the Padé factors are widened (that is, the value of c_P is increased) or, equivalently, when the molecules are left to move more freely around the equilibrium positions, the energy of the system increases. Given the variational equivalency between $g_G(r)$ and $g_P(r)$, we opt for ψ_{NJ} with Gaussian factors and optimal parameters $b_G = 3.45$ Å and $a_G = 0.67$ Å^{-2} in our subsequent DMC calculations.

It is well known that ψ_{NJ} is not symmetric under the permutation of particles [that is, $\psi_{NJ}(\mathbf{r}_1, \mathbf{r}_2, \ldots, \mathbf{r}_N) \neq \psi_{NJ}(\mathbf{r}_2, \mathbf{r}_1, \ldots, \mathbf{r}_N)$]. This property is manifestly incorrect for a system of indistinguishable bosons. Nevertheless, the use of the Nosanow-Jastrow model is widely spread within the field of microscopic calculations since it is assumed that the effect of symmetrization on the total and partial energies of quantum solids is practically negligible. In fact, we will show in brief that this is also the case for two-dimensional

TABLE I. Optimal variational total energy per particle obtained at the density $\rho=0.060$ Å^{-2} with different trial-wave-function models. Values appearing on the left (right) side of the table correspond to one-body factors $g_1(r)$ adopted in the form $g_G(r)$ $[g_P(r)]$.

	b_G (Å)	a_G (Å^{-2})	E/N (K)	Q_2 (%)	b_P (Å)	a_P (Å^{-2})	c_P (Å^{-1})	E/N (K)	Q_2 (%)
ψ_{NJ}	3.45	0.67	−21.3(1)		3.32	0.46	0.20	−21.3(1)	
ψ_{JL}^{S1}	3.45	0.67	−21.3(1)	4×10^{-3}	3.32	0.46	0.20	−21.3(1)	6×10^{-2}
ψ_{JL}^{S2}	3.58	0.38	−17.9(1)		3.70	0.69	0.39	−17.9(1)	
ψ_{JG}^{S3}	3.45	0.61	−20.4(1)						

hydrogen. To this end, we have tested the quality of several symmetrized trial wave functions in the variational study of 2D solid p-H_2. As mentioned in Sec. I, our motivation for this analysis is twofold: estimate the influence in the energy of molecular quantum exchanges and chiefly study the possibility of its use as importance sampling in DMC to determine the possible existence of BEC and superfluidity.

We have studied three different symmetrized trial wave functions. The first model consists in a permanent of monoparticular functions containing the $N!$ possible permutations $\{P\}$ of the N particles among the different lattice sites, expressed as

$$\psi_{JL}^{S1}(\mathbf{r}_1,\mathbf{r}_2,\ldots,\mathbf{r}_N)=\psi_J\sum_{\{P\}}\prod_{i=1}^{N}g_1(\mathbf{r}_i-\mathbf{R}_{Pi}). \tag{9}$$

Due to the algebraic difficulties arising in the implementation of permanents (contrarily to what occurs with determinants), the sampling of ψ_{JL}^{S1} must be divided into two different parts, one performed in the space of spatial configurations and the other in the space of permutations.[26] The acceptance probability for a proposed change in position of the particle labeled i, $\mathbf{r}_i\rightarrow\mathbf{r}_i'$, corresponds to

$$q=\min\left(1,\frac{\psi_J(\mathbf{r}')^2 g_1(\mathbf{r}_i'-\mathbf{R}_i)g_1(\mathbf{r}_i'-\mathbf{R}_{Pi})}{\psi_J(\mathbf{r})^2 g_1(\mathbf{r}_i-\mathbf{R}_i)g_1(\mathbf{r}_i-\mathbf{R}_{Pi})}\right), \tag{10}$$

where the subindex Pi can take any of the N possible lattice sites. On the other side, the acceptance probability for a proposed site permutation between the i and the j particles, $\mathbf{R}_{Pi}\leftrightarrow\mathbf{R}_{Pj}$, is

$$Q_2=\min\left(1,\frac{g_1(\mathbf{r}_j-\mathbf{R}_{Pi})g_1(\mathbf{r}_i-\mathbf{R}_{Pj})}{g_1(\mathbf{r}_j-\mathbf{R}_{Pj})g_1(\mathbf{r}_i-\mathbf{R}_{Pi})}\right). \tag{11}$$

Notice that permutations involving more than two particles are not sampled since the acceptance level for swap permutations is already extremely low.

The optimal results obtained with ψ_{JL}^{S1}, using Gaussian and Padé $g_1(r)$ functions, are reported in Table I. By comparing the variational energies obtained with ψ_{NJ} and ψ_{JL}^{S1}, we show that symmetrizing ψ_{NJ} with the above prescription has not appreciable effects on the total energy of p-H_2. Nevertheless, it must be said that one should not draw other conclusive statements about the effects of a full symmetrization just based on the approximation of the permanent by a reduced sampling in the permutation space of type (11). In fact, the acceptance rate of permutations is so low (column Q_2 in Table I) that sampling ψ_{JL}^{S1} efficiently turns out to be quite challenging.

The second model of symmetrized trial wave function ψ_{JL}^{S2} consists in a productory of sums in the form

$$\psi_{JL}^{S2}(\mathbf{r}_1,\mathbf{r}_2,\ldots,\mathbf{r}_N)=\psi_J\prod_{i=1}^{N}\left(\sum_{j=1}^{N}g_1(\mathbf{r}_i-\mathbf{R}_j)\right). \tag{12}$$

This trial wave function has been proposed very recently by Zhai and Wu[27] and has been suggested to be of possible relevance for the study of the supersolid. In fact, ψ_{JL}^{S2} avoids any explicit sampling in permutation space hence turns out to be well suited for being used as importance sampling in DMC simulations. However, as one can see in Table I the best variational energy obtained with this model is sizably larger than the ones obtained with ψ_{NJ} and ψ_{JL}^{S1} in both Gaussian and Padé cases. In fact, the variational energy obtained with ψ_{JL}^{S2} is very similar to the one calculated with ψ_J for the liquid ($\sim$−17.4 K). In doing the simulation with this wave function it is observed that particles diffuse excessively within the container giving place to glassylike configurations; we have checked this feature by monitoring the radial pair distribution function (see Fig. 2) and mean squared displacement (which grows steadily with time). The reason for this excessive atomic diffusion is that the way in which the one-body factor is symmetrized in ψ_{JL}^{S2} does not penalize

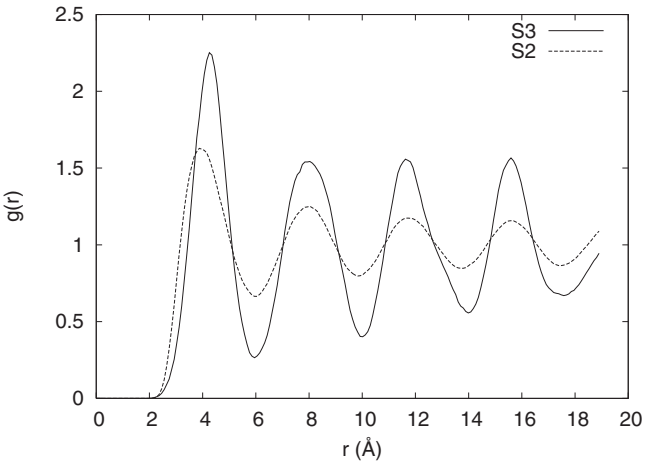

FIG. 2. Variational radial pair distribution function $g(r)$ of two-dimensional molecular hydrogen at the density $\rho=0.060$ Å^{-2} obtained with TWFs ψ_{JG}^{S2} and ψ_{JG}^{S3}.

multiple occupation of a same lattice site. This feature will be illustrated in short by means of a simple example involving two particles moving in one dimension. Moreover, if the width of $g_1(r)$ is narrowed in order to avoid such unrealistic molecular diffusion, the total energy of the system is worsened because of the rapid increase in kinetic energy.

The third type of symmetrized trial wave function reads

$$\psi_{JG}^{S3}(\mathbf{r}_1,\mathbf{r}_2,\ldots,\mathbf{r}_N) = \psi_J \prod_{j=1}^{N} \left(\sum_{i=1}^{N} g_1(\mathbf{r}_i - \mathbf{R}_j) \right), \qquad (13)$$

and it is also straightforward to implement in DMC codes. This type of trial wave function has been proposed very recently by Cazorla *et al.*[23] and has been used to set an upper bound of 10^{-5} for the superfluid fraction of perfect crystalline bulk ^{4}He at zero temperature. ψ_{JG}^{S3} and ψ_{JG}^{S2} look similar, the difference being that the productory and summatory in ψ_{JG}^{S3} run over sites and particles, respectively, while in ψ_{JG}^{S2} is the other way around. However, ψ_{JG}^{S3} and ψ_{JG}^{S2} lead to completely different variational energies (see Table I). The best variational result obtained with ψ_{JG}^{S3} amounts to −20.4(1) K, which is only 0.9 K larger than the one calculated with ψ_{NJ} or ψ_{JL}^{S1} but 2.5 K smaller than the one corresponding to ψ_{JG}^{S2}. In this case, the radial pair distribution function and mean squared displacement follow typical solidlike patterns (see Fig. 2).

Contrary to what occurs with ψ_{JG}^{S2}, the multiple occupation of the same site is now penalized by the wave function and hence crystal order is sustained. To the end of illustrating this feature, which appears to be the main difference between ψ_{JG}^{S2} and ψ_{JG}^{S3}, we have analyzed the simple case of two particles moving in a one-dimensional lattice. For the sake of simplicity, we have assumed that the distance between the equilibrium positions of the particles is 1, the parameter entering the Gaussian factors in Eqs. (9) and (13) is $a=1/2$, in arbitrary units (arb. units), and that the Jastrow factor is switched off ($\psi_J=1$). The value of the squared wave function for ψ_{JG}^{S2} and ψ_{JG}^{S3}, $|\psi_{\mathrm{sol}}|^2$, obtained by keeping fixed one of the particles in the site located at the origin and then moving the other particle toward it, is plotted in Fig. 3 for the interval $0 \le x \le 1$. As one observes in there, the value of ψ_{JG}^{S2} at $x=1$ and 0 (that is, each particle is placed over one site or both are at the same position, respectively) is the same, whereas $\psi_{JG}^{S3}(x=1) > \psi_{JG}^{S3}(x=0)$. This effect is what we have previously referred to as "penalized by the trial wave function." It is also noted that the value of ψ_{JG}^{S2} is maximum at half the way between 0 and 1, not so for ψ_{JG}^{S3}, hence ψ_{JG}^{S2} will always promote larger diffusion of the molecules.

B. Diffusion Monte Carlo results

We have studied the energetic and structural properties of p-H_2 using the DMC method and ψ_{NJ} (6) as trial wave function. We have verified that the DMC energy and diagonal properties obtained with ψ_{NJ} are statistically indistinguishable from the ones obtained using the symmetric wave function ψ_{JG}^{S3} (13). The results presented in this section have been obtained for a rectangular plane containing 90 particles with periodic boundary conditions in the two spatial directions.

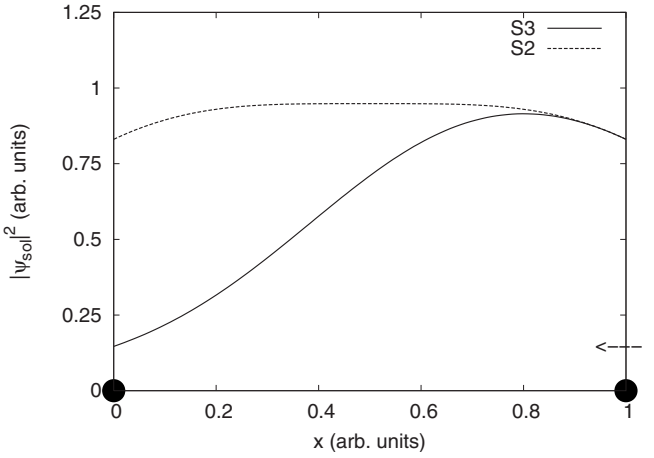

FIG. 3. Squared ψ_{JG}^{S2} and ψ_{JG}^{S3} (with $\psi_J=1$) in the simple case of two particles moving in one dimension and sites separated by one arbitrary unity.

Internal parameters of the simulations, namely, the averaged population of walkers and time step, are 250 and 5×10^{-4} K^{-1}, respectively; these parameters have been adjusted in order to reduce any possible bias to the level of the statistical uncertainty (∼0.05 K).

In Table II, we report the total ground-state energy per particle, E/N, corresponding to 2D solid p-H_2 at some densities. The pure (unbiased) estimations of the potential, V/N, and kinetic energies, T/N, are also quoted therein. The energy results have been corrected for the finite size of the simulation plane by assuming the radial pair distribution function $g(r)$ to be one beyond the distance $R_{\max}=L/2$, with L being the size of the plane. Assuming $g(r) \sim 1$ beyond $R_{\max}$ could seem a crude approximation for crystals since this function shows periodic structure (see, for instance, Fig. 5). However, the periodic oscillations of $g(r)$ around unity might suggest that in average this approximation is essentially correct. In order to test the reliability of this finite-size correction we have calculated the total energy per particle in a plane containing 90, 120, and 168 molecules at the density $\rho=0.0597$ Å^{-2}; we obtain $E/N=-22.19(2)$, −22.16(2), and −22.15(2) K, respectively, thus achievement of convergence within the present statistical uncertainty is proved.

The energy per particle corresponding to liquid and solid 2D p-H_2 at zero temperature is plotted in Fig. 4 as a function

TABLE II. Ground-state energy E/N, potential energy V/N, and kinetic energy T/N per particle of solid 2D p-H_2. Potential and kinetic energies are obtained with pure estimators.

ρ (Å^{-2})	E/N (K)	V/N (K)	T/N (K)
0.053	−19.42(2)	−35.73(3)	16.30(3)
0.060	−22.21(2)	−43.67(3)	21.46(3)
0.065	−23.27(2)	−49.23(4)	25.96(4)
0.067	−23.42(2)	−51.68(4)	28.26(4)
0.070	−23.19(2)	−54.83(4)	31.64(4)
0.076	−21.30(2)	−59.22(5)	37.92(5)
0.083	−14.23(2)	−62.40(7)	48.17(7)

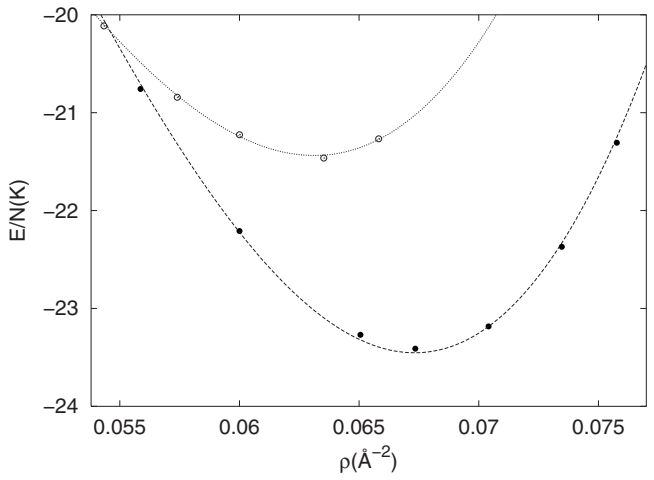

FIG. 4. Total ground-state energy per particle of liquid (dotted line) and solid (dashed line) 2D p-H_2 at zero temperature. The lines correspond to polynomial fits of our results (empty and filled circles); the statistical error bars are smaller than the symbol size.

of the density. The simulation of the metastable liquid phase uses a Jastrow wave function ψ_J (5) as importance sampling. The lines in Fig. 4 correspond to polynomial fits to our results in the form

$$E/N = e(\rho) = e_0 + B\left(\frac{\rho-\rho_0}{\rho_0}\right)^2 + C\left(\frac{\rho-\rho_0}{\rho_0}\right)^3. \quad (14)$$

The pressure, compressibility, and speed of sound (averaged for all the directions) are then easily derived from Eq. (14) through the expressions

$$P(\rho) = \rho^2 \frac{\partial e(\rho)}{\partial \rho}, \quad (15)$$

$$\kappa(\rho) = \frac{1}{\rho}\left(\frac{\partial \rho}{\partial P}\right)_T, \quad (16)$$

$$c(\rho) = \left(\frac{1}{m\kappa\rho}\right)^{1/2}. \quad (17)$$

The optimal values of the parameters for the solid phase are e_0=−23.453(3) K, ρ_0=0.0673(2) Å^{-2}, B=121(2) K, and C=152(8) K, where e_0 and ρ_0 are the equilibrium energy per particle and density, respectively. According to these figures, the compressibility and speed of sound at the equilibrium density are $\kappa(\rho_0)$=0.0615(8) Å^2/K and $c(\rho_0)$ =998.6(1) m/s, the numbers quoted within parentheses being the statistical errors. The equation of state of the liquid phase is also well described by the polynomial form (14) with optimal parameters e_0=−21.43(2) K, ρ_0 =0.0633(3) Å^{-2}, B=75(7) K, and C=69(9) K.

Another magnitude of interest in the study of bulk systems is the spinodal density ρ_S. ρ_S sets the limit for the system to remain in a homogeneous phase since at this density the compressibility grows to infinite (or equivalently, the speed of sound becomes zero); in case of going below this point ($\rho < \rho_S$) the system breaks down into clusters. According to our DMC calculations, this low-limit density amounts to ρ_S=0.0548(1) Å^{-2} in solid p-H_2.

A glance at Fig. 4 shows that the solid phase is the stable one overall the regime of positive pressures. Nevertheless, by looking at our results one could suggest a first-order liquid-solid phase transition occurring at negative pressures, where the two equations of state cross each other. Needless to be said that this possibility deserves detailed exploration since it could provide a chance for superfluidity to be observed in a quantum liquid different from helium. Aimed at this, we have simulated 2D liquid p-H_2 down to densities of 0.039 Å^{-2} [the spinodal density of the liquid is ρ_S =0.0519(1) Å^{-2}] and searched for that transition by means of the Maxwell double-tangent construction. Our results show that a liquid-solid transition is not possible within the range set by the spinodal densities, and thus the possibility of liquid p-H_2 in two dimensions must be rejected.

Our results for the equation of state of p-H_2 can be compared with two previous path-integral Monte Carlo (PIMC) studies carried out on the same system. In Ref. 28, Gordillo and Ceperley obtained ρ=0.064 Å^{-2} for the equilibrium density of 2D solid p-H_2 at T=1 K; the authors of that work reported a figure with the energy per particle as a function of the density, and the minimum of the curve is located at ∼ −22.0 K. A more systematic analysis of the same system was performed later on by Boninsegni.[29] In that work, the total energy per particle and chemical potential are calculated at several densities and within the temperature range T =1–8 K. Subsequently, an extrapolation of the low temperature results to absolute zero was performed, leading to ρ_0^{PIMC}=0.0668(5) Å^{-2}, e_0^{PIMC}=−23.25(5) K, and ρ_S^{PIMC} =0.0585(10) Å^{-2}. We note that the agreement between those zero-temperature extrapolated PIMC values and our DMC results is fairly good, especially in the case of the equilibrium density ρ_0.

We have analyzed the structure of the 2D solid by calculating the radial pair distribution function $g(r)$,

$$g(r) = \frac{N-1}{\rho}\frac{\int |\Psi(\mathbf{r}_1, \mathbf{r}_1+\mathbf{r}, \ldots, \mathbf{r}_N)|^2 d\mathbf{r}_1 d\mathbf{r}_3 \ldots d\mathbf{r}_N}{\int |\Psi(\mathbf{r}_1, \mathbf{r}_2, \ldots, \mathbf{r}_N)|^2 d\mathbf{r}_1 \ldots d\mathbf{r}_N}, \quad (18)$$

and Lindemann's ratio γ_{H_2},

$$\gamma = \frac{1}{a}\sqrt{\left\langle \frac{1}{N}\sum_{i=1}^{N} (\mathbf{r}_i - \mathbf{R}_i)^2 \right\rangle} = \frac{\langle \mathbf{u}^2 \rangle^{1/2}}{a}, \quad (19)$$

where a is the distance between nearest neighbors in the perfect crystalline configuration. In Fig. 5, we plot $g(r)$ at the density 0.068 Å^{-2} which, as it is expected in crystals, exhibits a pattern of periodic order. At low temperatures, Lindemann's ratio γ around the equilibrium density tends to zero in classical solids while in quantum crystals it is finite due to the zero-point motion of particles; hence this quantity is regarded as a good quantum indicator. Furthermore, Linde-

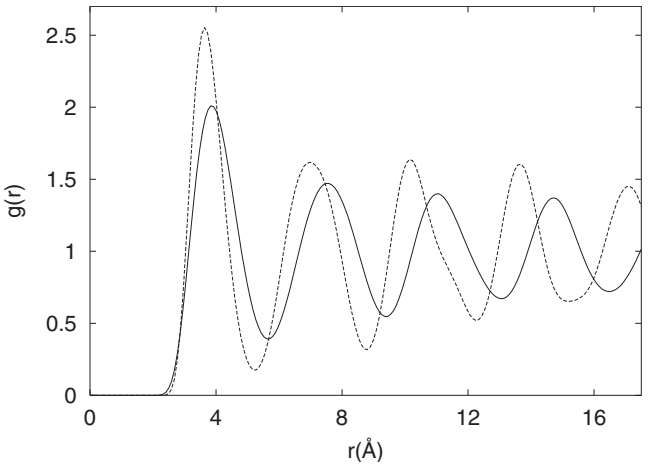

FIG. 5. Radial pair distribution functions of 2D solid o-D_2 at the equilibrium density $\rho_0=0.078$ Å^{-2} (dashed line) and of p-H_2 at the density 0.068 Å^{-2} (solid line).

mann's ratio (or equivalently, the mean squared displacement) is related to the Debye-Waller factor M_Q, which describes the attenuation of the emergent radiation in coherent scattering experiments according to the formula $I(Q,T) \propto e^{(-2M_Q)}$ [where $I(Q,T)$ is the intensity of the outgoing radiation scattered by the target and Q is the modulus of the transfer wave vector]. By means of a cumulant expansion, the Debye-Waller factor can be expressed as

$$2M_Q = \langle u_Q^2 \rangle Q^2 - \frac{1}{12}(\langle u_Q^4 \rangle - 3\langle u_Q^2 \rangle^2)Q^4 + O(Q^6), \quad (20)$$

where $\langle u_Q^2 \rangle$ is the mean squared displacement along the direction $\hat{\mathbf{Q}}$. It is easy to see that when the distribution of particles around the equilibrium positions is well described by a Gaussian function, the quantity within parentheses in the second right term of Eq. (20), known as kurtosis ζ_Q, vanishes. In such a case, the Debye-Waller factor reduces to the simple formula $2M_Q=\langle u_Q^2 \rangle Q^2$. In Table III, we report Lindemann's ratio, kurtosis, and mean squared displacement of two-dimensional p-H_2 at different densities. We have calculated $\langle u_Q^2 \rangle$ and ζ_Q along two orthogonal directions and not found appreciable differences in the results. Moreover, the kurtosis is null in all the studied cases. Consequently, we may conclude that the distribution of hydrogen molecules around the equilibrium positions is isotropic and can be accurately reproduced by a Gaussian, contrary to what is found to occur in ^{4}He.[30] Regarding the value of γ, it can be said that solid H_2 is *less* quantum than ^{4}He since $\gamma_{H_2} \sim 0.18$ at ρ_0 whereas in solid helium $\gamma_{He} \sim 0.24$ near melting.[7] Also it is worth noticing that the trend of γ_{H_2} is to increase with decreasing density; therefore quantum exchange effects in the crystal would become of greater relevance at small densities.

TABLE III. Lindemann's ratio γ_{H_2}, kurtosis ζ, and mean squared displacement $\langle \mathbf{u^2} \rangle$ of 2D solid p-H_2 at different densities close to equilibrium (pure estimations).

ρ (Å^{-2})	γ_{H_2}	$\zeta_{(10)}$	$\zeta_{(01)}$	$\langle \mathbf{u^2} \rangle$ (Å^2)
0.058	0.212(1)	0.00(2)	0.00(2)	0.19(1)
0.060	0.197(1)	0.02(2)	0.00(2)	0.15(1)
0.065	0.183(1)	0.02(2)	0.02(3)	0.12(1)
0.067	0.178(1)	−0.01(1)	−0.02(2)	0.11(1)
0.070	0.170(1)	−0.02(1)	0.00(2)	0.09(1)
0.076	0.158(1)	0.00(2)	0.01(1)	0.07(1)
0.083	0.146(1)	0.01(2)	0.01(1)	0.06(1)

IV. MOLECULAR *ORTHO*-DEUTERIUM

The ground-state properties of o-D_2 (with zero total angular momentum) have also been studied using the DMC method and the same radial pair potential (Silvera-Goldman[12]) as in p-H_2. The larger mass of D_2 makes one to expect that two-dimensional bulk D_2 is solid at zero temperature, so in this case we have restricted our study to the solid phase.

In our simulations, the equilibrium positions of the o-D_2 molecules are arranged according to a triangular lattice and the particles are assumed pointlike. In this case, we use the trial wave function,

$$\psi'_{NJ}(\mathbf{r}_1,\mathbf{r}_2,\ldots,\mathbf{r}_N) = \prod_{i<j}^{N} e^{-(1/2)(b/r_{ij})^c} \prod_{i}^{N} e^{-(a/2)(|\mathbf{r}_i-\mathbf{R}_i|)^2}, \quad (21)$$

which differs slightly from ψ_{NJ} in Eq. (6) (now the pair-correlation factors f_2 depend on the extra variational parameter c). The variational parameters in Eq. (21) have been optimized using VMC; the best values are $b=3.32$ Å, $c=7$, and $a=0.67$ Å^{-2}. All the DMC simulations have been performed in a rectangular plane containing 120 particles and applying periodic boundary conditions. The target averaged population of walkers, n_w, is 250 and the time step, $\Delta\tau$, is 5×10^{-4} K^{-1}. Finite size effects have been corrected with the same approach than used for hydrogen (see Sec. III B).

In Fig. 6, we plot the total ground-state energy per o-D_2 molecule as a function of the density; the solid line represents the best fit to our data following the polynomial function expressed in Eq. (14). The best values of the parameters are $B=241(3)$ K, $C=324(10)$ K, $e_0=-42.305(5)$ K, and $\rho_0=0.0785(2)$ Å^{-2}, which lead to a spinodal density $\rho_S=0.0641(2)$ Å^{-2}. By comparing with p-H_2, we show that o-D_2 is denser at equilibrium and appreciably more bounded (the total energy decreases substantially). The heavier mass of the o-D_2 molecules makes the solid to reduce its kinetic energy and mean squared displacement at any density (see Tables II–V), thus allowing the system to increase its equilibrium density in order to take advantage of the attractive interparticle interaction.

Concerning the structural properties of 2D solid o-D_2, we have calculated the radial pair distribution function at the equilibrium density (see Fig. 5) and Lindemann's ratio and kurtosis at different points (see Table V). As it is shown in Fig. 5, the peaks of the radial pair distribution function of 2D o-D_2 are sharper and somewhat closer than in molecular hy-

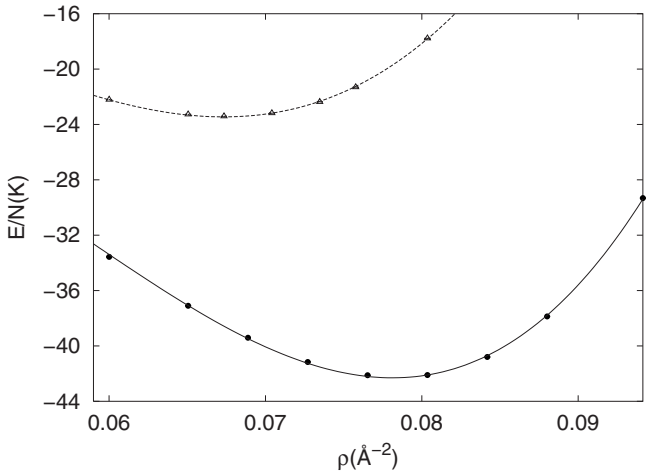

FIG. 6. Ground-state energy per particle of 2D solid o-D_2 (solid line and filled circles) and 2D solid p-H_2 (dotted line and empty triangles) which is shown for comparison.

drogen at equilibrium since the density and degree of localization of the particles are larger in the first case. This statement is also corroborated by the results contained in Table V, where Lindemann's ratio is invariably some tenths smaller than in p-H_2 at the same density. As a matter of comparison, Lindemann's ratio of o-D_2 at equilibrium is about 1.3 times smaller than that of p-H_2 and 1.7 than in two-dimensional ^{4}He. Furthermore, as it could be expected from our previous study of 2D p-H_2 (Table II), the kurtosis in two-dimensional o-D_2 is practically null in both the two orthogonal directions for which it has been calculated.

V. ONE-BODY DENSITY MATRIX AND OFF-DIAGONAL LONG-RANGE ORDER

A fundamental function in the study of quantum systems is the one-body density matrix $\varrho_1(\mathbf{r},\mathbf{r}')$, defined as

$$\varrho_1(\mathbf{r},\mathbf{r}') = \langle \Phi_0 | \hat{\psi}^\dagger(\mathbf{r}) \hat{\psi}(\mathbf{r}') | \Phi_0 \rangle, \tag{22}$$

where $\hat{\psi}(\mathbf{r}')$ and $\hat{\psi}^\dagger(\mathbf{r})$ are, respectively, the field operators which destroy a particle from position $\mathbf{r}'$ and create another at position $\mathbf{r}$ and Φ_0 is the ground-state wave function. In particular, a finite value for $\lim_{r\to\infty} \varrho_1(r)$ proves the existence of off-diagonal long-range order (ODLRO) in the system, the result being the condensate fraction n_0. In quantum Monte Carlo, the one-body density matrix can be estimated by averaging the coordinate operator $\psi_T(\mathbf{r}_1+\mathbf{r},\mathbf{r}_2,\ldots,\mathbf{r}_N)/\psi_T(\mathbf{r}_1,\mathbf{r}_2,\ldots,\mathbf{r}_N)$; here, we use extrapolated estimators for ϱ_1 since the pure estimation relying on forward walking is only applicable to diagonal operators. In order to get consistent results we have required that the two extrapolated estimators of the same accuracy, i.e., $\varrho_1(r) = 2\varrho_1^{\mathrm{mix}}(r) - \varrho_1^{\mathrm{var}}(r)$ and $\varrho_1(r) = [\varrho_1^{\mathrm{mix}}(r)]^2/\varrho_1^{\mathrm{var}}(r)$ (where *mix* means obtained with DMC and *var* with VMC), coincide within the present statistical uncertainty.

In Fig. 7, we compare DMC results for the one-body density matrix (ρ=0.060 Å^{-2}) obtained within the distance range $0<r<5.0$ Å and with both ψ_{NJ} (unsymmetrized) and ψ_{JG}^{S3} (symmetrized) trial wave functions. As can be observed, the series of points obtained with both TWFs is compatible in the full depicted range. In the same graph, we also enclose the Gaussian curve $G(r)=e^{-br^2}$ which best fits to the result obtained with ψ_{NJ}; we find that the best value of the parameter b is 0.400(6) Å^{-2}. In order to test the quality of this fit (which in the reduced chi-squared test leads to the value

TABLE IV. Ground-state total and pure potential and kinetic energies per particle of 2D o-D_2 at several densities.

ρ (Å^{-2})	E/N (K)	V/N (K)	T/N (K)
0.046	−22.40(2)	−29.84(3)	7.44(3)
0.053	−27.97(1)	−37.70(3)	9.73(3)
0.060	−33.57(1)	−46.38(4)	12.81(4)
0.069	−39.41(1)	−57.52(3)	18.11(3)
0.076	−42.12(1)	−66.46(6)	24.34(6)
0.084	−40.80(1)	−72.59(6)	31.79(6)
0.094	−29.32(2)	−73.18(8)	43.86(8)

TABLE V. Lindemann's ratio γ_{D_2} and kurtosis ζ of two-dimensional o-D_2 at different densities near the equilibrium.

ρ (Å^{-2})	γ_{D_2}	$\zeta_{(10)}$	$\zeta_{(01)}$
0.053	0.204(1)	0.00(1)	−0.06(2)
0.060	0.187(1)	0.01(1)	0.00(1)
0.069	0.160(1)	0.00(2)	−0.01(1)
0.073	0.149(1)	−0.01(1)	0.01(1)
0.078	0.139(1)	0.00(1)	0.01(1)
0.080	0.135(1)	−0.02(1)	0.00(1)
0.088	0.124(1)	0.00(1)	−0.03(1)
0.094	0.117(1)	−0.02(1)	0.02(1)

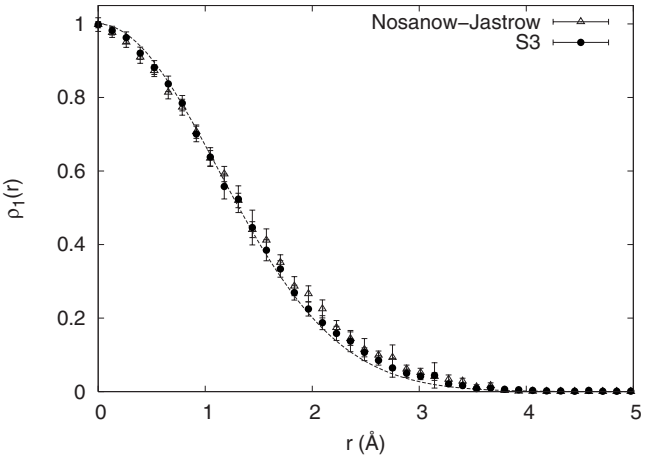

FIG. 7. One-body density matrix of p-H_2 $\varrho_1(r)$ obtained using as importance sampling ψ_{NJ} and ψ_{JG}^{S3} at the density ρ=0.060 Å^{-2}. The solid line corresponds to the Gaussian function which best fits to the Nosanow-Jastrow result.

1.59), we have calculated the atomic kinetic energy of two-dimensional p-H_2 through the formula

$$T/N = -\left[\frac{\hbar^2}{2m_{H_2}}\nabla^2\varrho_1(r)\right]_{r=0}, \tag{23}$$

but assuming $G(r)$ instead of $\varrho_1(r)$. In fact, it may be shown that Eq. (23) derives from the second moment of the momentum distribution $n(k)$,

$$T/N = \frac{\hbar^2}{2m_{H_2}}\frac{1}{(2\pi)^2\rho}\int d\mathbf{k}k^2 n(k). \tag{24}$$

Proceeding in this way, we obtain $T/N=19.40(30)$ K which does not agree satisfactorily with the corresponding pure (mixed) estimation 21.46(3) [20.75(2)] K. Very interestingly, Withers and Glyde[31] recently showed by means of simple models that anharmonic and/or particle-exchange effects in quantum solids may cause the momentum distribution $n(\mathbf{k})$ or equivalently $\varrho_1(r)$ to deviate significantly from a Gaussian function. Therefore, on account of our variational results reported in Sec. III A which show that molecule exchanges are likely to occur at very low rate, it may be suggested that two-dimensional hydrogen presents some degree of anharmonicity.

In Fig. 8 (a), we show DMC results similar to those enclosed in Fig. 7 but for larger distances and expressed in logarithmic scale in order to obtain the asymptote of ϱ_1. As one observes, the value of $\lim_{r\to\infty}\varrho_1$ in the unsymmetrized case tends obviously to zero while for ψ_{JG}^{S3} it amounts to a small but finite value $n_0=6(1)\times10^{-4}$. In the same figure (b), we compare $\varrho_1(r)$ at several densities and only for the symmetric wave function; we obtain $n_0=2(1)\times10^{-4}$ and $8(1)\times10^{-3}$ at the density 0.067 and 0.056 Å^{-2}, respectively. At the equilibrium density, we have performed a further test in order to assess any possible bias in our estimation of n_0. The test consists in computing $\varrho_1(r)$ with trial wave function ψ_{JG}^{S3} but using Padé functions g_P instead of Gaussian functions g_G as localizing factors g_1 [see Eq. (13)]. We have proceeded so and obtained $n_0=7(2)\times10^{-4}$ to be compared with $2(1)\times10^{-4}$. As one can see, both results are fairly compatible though not identical. In view of this outcome, it can be argued that despite the value of n_0 that we provide cannot be considered completely free of bias the corresponding order of magnitude is essentially correct.

Apart from the fact that we obtain a small but finite condensate fraction for the ground state of solid p-H_2 in two dimensions, we note that the value of n_0 raises very abruptly in moving from equilibrium to densities close to the spinodal point (where $P<0$). In a very recent work, we have analyzed the superfluid nature of solid ^{4}He at zero temperature by means of ψ_{JG}^{S3}.[23] In that work, we showed that the superfluid fraction of bulk solid ^{4}He lies below 1×10^{-5}, whereas a clear superfluid signal of $\rho_s/\rho=3.2(1)\times10^{-3}$ appears in the presence of 1% of vacancies. In the case of vacancies, we found that the condensate fraction increased by roughly a factor of 2 with respect to that of the perfect-crystal configuration. According to this previous result, a significant increase in n_0 in our simulations may be identified to the appearance of superfluidity in the system. Therefore, two-dimensional solid hydrogen is likely to become superfluid at very low coverages and temperatures. In fact, the superfluid density of a bosonic system can be calculated with DMC in an unbiased way by extending the winding-number technique, originally developed for PIMC calculations, to zero temperature.[32] Explicitly,

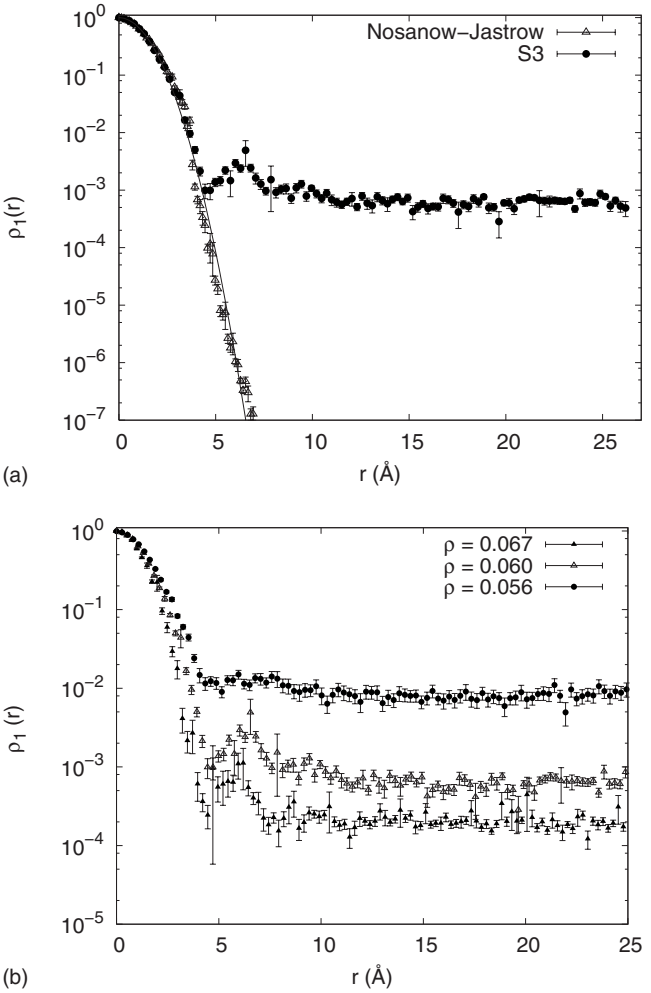

FIG. 8. (a) One-body density matrix of p-H_2 at density $\rho=0.060$ Å^{-2} obtained using importance sampling with the Nosanow-Jastrow and ψ_{JG}^{S3} trial wave functions. (b) One-body density matrix of p-H_2 obtained with the ψ_{JG}^{S3} trial wave function at several densities. Densities are in units of Å^{-2}.

$$\frac{\rho_s}{\rho} = \lim_{\tau\to\infty}\alpha\left(\frac{D_s(\tau)}{\tau}\right), \tag{25}$$

where $\alpha=N/4D_0$ with $D_0=\hbar^2/2m$ and $D_s(\tau)=\langle[\mathbf{R}_{CM}(\tau)-\mathbf{R}_{CM}(0)]^2\rangle$ with $\mathbf{R}_{CM}$ as the center of mass of the particles in the simulation box. Motivated by our results for n_0, we have carried out a series of simulations for estimating ρ_s/ρ in solid p-H_2; we find that at equilibrium ρ_s/ρ is null (or, more precisely, $\rho_s/\rho<10^{-5}$ which corresponds to our accuracy threshold), while at $\rho=0.060$ and 0.056 Å^{-2} ρ_s/ρ amounts to 0.28(1)% and 3.8(1)%, respectively.

In order to ensure that the significant raise of n_0 and appearance of superfluidity observed in our simulations are not

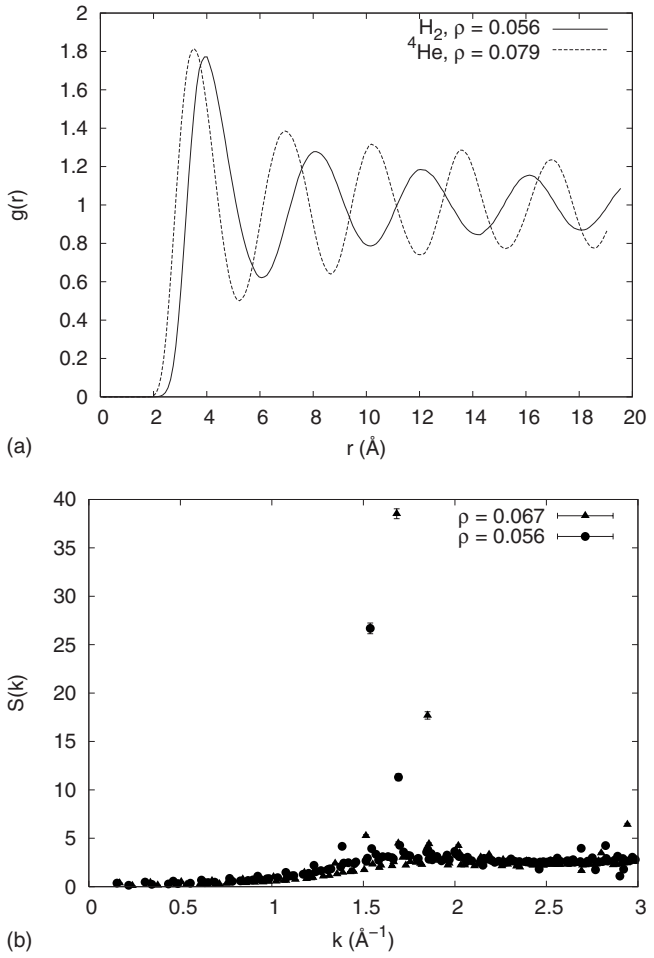

FIG. 9. (a) Radial pair distribution function of two-dimensional H_2 and ^{4}He near the spinodal and freezing densities, respectively. (b) Structure factor $S(k)$ of 2D H_2 at equilibrium density ρ_0 and $\rho=0.056$ Å^{-2}.

due to partial melting of H_2, we have calculated the corresponding radial pair distribution function at the density 0.056 Å^{-2}. In Fig. 9(a), we report $g(r)$ for hydrogen and compare it with the one obtained for two-dimensional ^{4}He above its freezing point. Clearly, a typical solid pattern emerges for H_2. Moreover, in 9(b) we also plot the structure factor $S(k)$ for molecular hydrogen at the equilibrium density $\rho_0=0.067$ Å^{-2} and $\rho=0.056$ Å^{-2}; in both cases marked peaks emerge at the reciprocal-lattice vectors. Therefore, the significant variation in n_0 and appearance of superfluid behavior with decreasing density are not caused by *a priori* guessed instabilities in the crystal.

VI. DISCUSSION AND CONCLUSIONS

To summarize, in this work we have studied two-dimensional p-H_2 and o-D_2 at zero-temperature and low pressures, with the diffusion Monte Carlo method and the Silvera-Goldman semiempirical pair interaction.[12] We have assessed several energetic and structural properties of both systems, such as the total and kinetic energy per particle, radial pair distribution function, and Lindemann's ratio, and quoted so isotopic quantum effects in hydrogen. Our results show that no stable liquid phase exists and therefore reducing one dimension with respect to bulk it is not enough to get the so longly searched superfluid phase of H_2.

Interestingly, Wiechert *et al.*[19] reported very recently on an experiment on molecular *ortho*-deuterium coadsorbed on graphite preplated by a layer of Kr up to temperatures of ~1.5 K. The authors of this work claim evidence for the existence of a reentrant D_2 liquid at very low temperatures based on their heat capacity and neutron-diffraction measurements. The system explored by Wiechert *et al.*[19] can be fairly modeled by a monolayer. However, on account of our results for H_2, the possibility of pure two-dimensional liquid deuterium at zero temperature must be ruled out. On the expectance of new and more explanatory experiments, we may point that, assuming that thermal effects are practically negligible, the role of the interactions between the deuterium molecules and the atoms of the substrate is the one of relevance. Certainly, Turnbull and Boninsegni[34] already addressed recent work on this direction by means of the PIMC method and simple interaction models.[33] Further improvement on the modeling of coadsorbed systems, putting special emphasis on the description of the interactions and the effect of corrugation with the substrate, may open new and challenging venues for the realization of superfluidity in p-H_2 and o-D_2 systems.[35]

At the variational level, we have analyzed the quality of three different symmetrized trial wave functions based on the Nosanow-Jastrow model in describing 2D solid molecular hydrogen. We have shown that the recently proposed symmetrized wave function used to describe the supersolid also characterizes solid hydrogen satisfactorily. By using that wave function, we have studied the behavior of the one-body density matrix of solid p-H_2 with density and predicted that the system becomes superfluid at very dilute densities (where $P<0$). At present, work aimed at understanding the origins of the predicted superfluid behavior of solid hydrogen at negative pressures is in progress.

ACKNOWLEDGMENTS

We acknowledge financial support from DGI (Spain) under Grant No. FIS2005-04181 and Generalitat de Catalunya under Grant No. 2005GR-00779.

[1] E. Kim and M. H. W. Chan, Science **305**, 1941 (2004).
[2] E. Kim and M. H. W. Chan, Nature (London) **427**, 225 (2004).
[3] S. Sasaki, R. Ishiguro, F. Caupin, H. J. Maris, and S. Balibar, Science **313**, 1098 (2006).
[4] Ann Sophie C. Rittner and J. D. Reppy, Phys. Rev. Lett. **97**, 165301 (2006).
[5] Ann Sophie C. Rittner and J. D. Reppy, Phys. Rev. Lett. **98**, 175302 (2007).
[6] E. Kim, J. S. Xia, J. T. West, X. Lin, A. C. Clark, and M. H. W. Chan, Phys. Rev. Lett. **100**, 065301 (2008).
[7] C. Cazorla and J. Boronat, J. Phys.: Condens. Matter **20**, 015223 (2008).
[8] C. Cazorla and J. Boronat, Phys. Rev. B **77**, 024310 (2008).
[9] B. L. Hammond, W. A. Lester, Jr., and P. J. Reynolds, *Monte Carlo Methods in Ab initio Quantum Chemistry* (World Scientific, Singapore, 1994).
[10] R. Guardiola, in *Microscopic Quantum Many-Body Theories and their Applications*, edited by J. Navarro and A. Polls (Springer, Berlin, 1998).
[11] D. M. Ceperley and M. H. Kalos, *Monte Carlo Methods in Statistical Physics* (Springer, Berlin, 1979).
[12] I. F. Silvera and V. V. Goldman, J. Chem. Phys. **69**, 4209 (1978).
[13] E. Babaev, A. Sudbo, and N. W. Ashcroft, Nature (London) **431**, 666 (2004).
[14] E. Babaev, A. Sudbo, and N. W. Ashcroft, Phys. Rev. Lett. **95**, 105301 (2005).
[15] M. C. Gordillo, J. Boronat, and J. Casulleras, Phys. Rev. Lett. **85**, 2348 (2000).
[16] R. Guardiola and J. Navarro, Phys. Rev. A **74**, 025201 (2006).
[17] S. A. Khairallah, M. B. Sevryuk, D. M. Ceperley, and J. P. Toennies, Phys. Rev. Lett. **98**, 183401 (2007).
[18] F. Mezzacapo and M. Boninsegni, Phys. Rev. Lett. **97**, 045301 (2006).
[19] H. Wiechert, K. D. Kortmann, and N. Stüsser, Phys. Rev. B **70**, 125410 (2004).
[20] K. S. Liu, M. H. Kalos, and G. V. Chester, Phys. Rev. A **10**, 303 (1974).
[21] P. J. Reynolds, R. N. Barnett, B. L. Hammond, and W. A. Lester, Jr., J. Stat. Phys. **43**, 1017 (1986).
[22] J. Casulleras and J. Boronat, Phys. Rev. B **52**, 3654 (1995).
[23] C. Cazorla, G. E. Astrakharchik, J. Casulleras, and J. Boronat, arXiv:0804.1851 (unpublished).
[24] M. H. Kalos, D. Levesque, and L. Verlet, Phys. Rev. A **9**, 2178 (1974).
[25] S. A. Chin, Phys. Rev. A **42**, 6991 (1990).
[26] D. Ceperley, G. V. Chester, and M. H. Kalos, Phys. Rev. B **17**, 1070 (1978).
[27] H. Zhai and Y.-S. Wu, J. Stat. Mech.: Theory Exp. 2005, P07003.
[28] M. C. Gordillo and D. M. Ceperley, Phys. Rev. Lett. **79**, 3010 (1997).
[29] M. Boninsegni, Phys. Rev. B **70**, 193411 (2004).
[30] E. W. Draeger and D. M. Ceperley, Phys. Rev. B **61**, 12094 (2000).
[31] B. Withers and H. R. Glyde, J. Low Temp. Phys. **147**, 633 (2007).
[32] S. Zhang, N. Kawashima, J. Carlson, and J. E. Gubernatis, Phys. Rev. Lett. **74**, 1500 (1995).
[33] M. Boninsegni, New J. Phys. **7**, 78 (2005).
[34] J. Turnbull and M. Boninsegni, Phys. Rev. B **76**, 104524 (2007).
[35] C. Cazorla and J. Boronat, J. Low Temp. Phys. **43**, 134 (2004).